IEEE Open Journal of Vehicular Technology

Received 20 September 2022; accepted 13 October 2022. Date of publication 19 October 2022;
date of current version 8 November 2022. The review of this article was coordinated by Editor Zhaocheng Wang.

Digital Object Identifier 10.1109/OJVT.2022.3215662

Radio-Protected Area Estimation Model Using Location-Dependent Gain for a Spectrum Sharing System in the VHF-Band

KEIKA MINAKI [1] (Student Member, IEEE), SOHEI YANASE[1], SHINGO TOMIDA[1], KEIICHI MIZUTANI [1,2] (Member, IEEE), AND HIROSHI HARADA [1] (Member, IEEE)

[1]Graduate School of Informatics, Kyoto University, Kyoto 606-8501, Japan
[2]School of Platforms, Kyoto University, Kyoto 606-8501, Japan

CORRESPONDING AUTHOR: HIROSHI HARADA (e-mail: hiroshi.harada@i.kyoto-u.ac.jp)

This work was supported by the Ministry of Internal Affairs and Communications in Japan, SCOPE under Grant JP196000002.

ABSTRACT This paper proposes a radio-protected area (RPA) estimation model that achieves full protection and avoids overprotection by adding an appropriate margin to the extended-Hata (EH) model, for realizing efficient spectrum sharing in the V-High-band. This additional margin, called location gain, is a location-dependent value that accounts for knife-edge losses calculated from topographic information. This study experimentally obtains the location gain by conducting VHF-band-based propagation experiments in urban and suburban areas. Subsequently, we developed an estimation formula for the location gain using topographic data, which include correction terms based on the experimental data. As a result, RPA can be estimated using only the topographic data, excluding the need for propagation experiments. The proposed model resolved the problems of the EH model (incomplete protection) and free-space (FS) model (overprotection). In urban and suburban areas, the proposed model achieved full protection and over 99.7% reduction in the RPA size of the FS model when the threshold of the received power for determining the RPA was set to –80 dBm.

INDEX TERMS Knife-edge loss, location-gain, radio-protected area, spectrum sharing, VHF.

I. INTRODUCTION

In Japan, terrestrial analog television (TV) broadcasting services at very high frequency (VHF) and ultra-high frequency (UHF) bands were terminated in 2012. Following this termination, 130 MHz of new spectrum resources were created for use by other communication systems [1]. The Ministry of Internal Affairs and Communications of Japan allocated 170–202.5 MHz (with 5 MHz bandwidth for each channel, six channels in total), as part of providing new spectral resources to public broadband (PBB) systems—mobile broadband wireless communication systems for public safety [1]. This spectral band is referred to as the PBB band.

The ARIB STD-T103 was developed as a domestic standard for Japanese PBB systems [2]. It is an orthogonal frequency division multiple access (OFDMA)-based standard developed based on the IEEE 802.16-2009 standard [3], with customized physical layer parameters for operability in the VHF band [3], [4], [5]. The relatively long wavelength of the VHF band permits longer transmission distances and a wide coverage area. However, it faced the issue of excessively delayed multipath fading. Therefore, a longer cyclic prefix (CP) than IEEE 802.16-2009, and a unique pilot signal alignment were defined in ARIB STD-T103 [3]. This allowed the ARIB STD-T103-based PBB system to provide high-quality video transmission and other broadband services, even in non-line-of-sight environments over a wide area. Furthermore, to realize a wider area coverage, ARIB STD-T119 was standardized to enable the operation of ARIB STD-T103 in the multi-hop relay communication mode [6], [7]. The development and commercialization of ARIB STD-T103/T119-based PBB systems are currently underway as critical wireless mobile communication infrastructure for public agencies (e.g., police, fire departments, emergency services, and local governments) during disasters and emergencies. These systems

This work is licensed under a Creative Commons Attribution 4.0 License. For more information, see https://creativecommons.org/licenses/by/4.0/

are expected to accommodate high-resolution video/image transmission communication by multiple public agency users at disaster emergency sites in the future. Furthermore, in addition to these public agencies, private institutions related to disaster recovery, such as electric power companies, demand the availability of VHF band-based communication. However, as only six channels (5 MHz bandwidth for each channel) can be allocated in the PBB band, more spectrum resource allocation is required to accommodate further increase in data traffic and user agencies.

The most promising candidate for an additional spectrum for the PBB system is the 207.5–222 MHz band called as the V-High-band. Similar to the PBB band, the V-High-band is part of the VHF band reallocation due to the termination of terrestrial analog TV broadcasting. Communications via mobile terminals for multimedia broadcasting services were allocated from 2012; however, all services were terminated in 2016 and the V-High-band became vacant again. Various systems, including the PBB systems, are currently candidates for V-High-band use systems, although no final operational guidelines have been determined. Considering the problem of spectrum resource depletion, there is a possibility that multiple systems will share the V-High-band spectrum.

Spectrum sharing systems have been studied and implemented as TV white space utilization systems (e.g., IEEE 802.11af [8], [9], [10], [11], IEEE 802.15.4m [12], [13], [14], and IEEE 802.22 [15], [16], [17]), licensed shared access (LSA) in Europe [18], [19], [20], spectrum access system (SAS) in the United States [21], [22], [23], and dynamic spectrum sharing (DSS) in Japan [24], [25], [26]. In these spectrum-sharing systems, a primary user with a high priority (such as a system originally allocated to the spectrum) and a secondary user with a low priority (such as a system newly allocated to the spectrum) share the same spectrum. Secondary users can use the spectrum only if they do not interfere with primary users or have a minor impact on them.

To perform interference estimations, system information such as location and transmit power of base stations (BSs) and mobile stations (MSs) for each system is registered in the spectrum-sharing database. Using this registered information and a radio propagation model such as the free-space (FS) model [27], the extended Hata (EH) model [28], the ITU-R P.1411 model [29], or the Walfish-Ikegami model [30], [31], the communication service area of each system is estimated. Among these models, the FS and EH models are available in the VHF band (around 200 MHz, the target band of this paper). The estimated area that should be protected from interference emitted by other systems is referred to as the *radio-protected area (RPA)* in this study. Intersystem interference can be prevented by adjusting the transmission parameters to avoid overlapping of the RPA for each system. However, conventional RPA estimation models are problematic from two perspectives: overprotection and incomplete protection. The FS model often overestimates the RPA, which is problematic in terms of spectral efficiency [32], while the EH model often underestimates the RPA as too small and cannot achieve full protection because the EH model is only an experimental model that mainly estimates average transmission characteristics [32], [33], [34]. To use the EH model as an RPA estimation model, a significant distance margin must be added to fully protect the primary user. This results in excessive protection even in areas that do not require protection (areas inherently available to secondary users), resulting in the degradation of spatial-spectral efficiency [32].

This paper proposes an RPA estimation model that achieves full protection and avoids overprotection to increase the available area for secondary users while fully protecting primary users from interference by adding an appropriate margin to the EH model, aiming for a highly efficient spectrum sharing realization in the V-High-band. This additional margin is a location-dependent value that accounts for the knife-edge losses [35] calculated from the topographic information, including building heights, and is referred to as the *location gain*. In this paper, the location gain was experimentally obtained by conducting VHF-band propagation experiments in urban and suburban areas. Subsequently, an estimation formula for location gain using topographic data, was developed, which included the correction terms based on the experimental data. Therefore, using our developed estimation formula, RPA can be calculated using only the topographic data, excluding the need for propagation experiments.

The remainder of this paper is organized as follows: Section II provides an overview of the conventional radio propagation models for RPA calculation. In Section III, RPA estimation is demonstrated using conventional radio propagation models by conducting actual radio propagation experiments in urban and suburban areas to highlight the problems with the conventional models and to clarify the motivation for this paper. In Section IV, the proposed methods are presented. Sections V and VI evaluate the proposed methods using actual propagation measurement data in an urban area and a suburban area, respectively. Finally, Section VII concludes this paper.

II. CONVENTIONAL MODELS FOR RPA ESTIMATION

In this section, we explain the typical radio propagation models for RPA estimation: the FS and EH models. In this study, the outermost side of the RPA is called the *protection boundary* and the distance from the BS to the protection boundary is called the *protection distance*.

A. FREE-SPACE MODEL (FS MODEL)

The FS model is the most basic radio propagation loss-calculation model. The propagation loss $L_{\mathrm{F}}(d)$ (dB) is expressed as follows:

$$L_{\mathrm{F}}(d) = 20\log_{10}d + 20\log_{10}f + 32.44 \tag{1}$$

where f (MHz) is the frequency and d (km) is the antenna distance between the BS and MS [27]. Here, we define the received power threshold for determining the RPA by P_{th} (dBm). In other words, received power greater than P_{th} is

not measured outside the RPA. Moreover, propagation loss is also determined at the protection boundary $L(P_{\text{th}})$, using the transmitting (Tx) power P_{t} (dBm) of the BS, Tx antenna gain G_{t} (dBi), receiving antenna gain G_{r} (dBi), and P_{th} as follows:

$$L\left(P_{\text{th}}\right) = P_{\text{t}} + G_{\text{t}} + G_{\text{r}} - P_{\text{th}}. \tag{2}$$

When the protection distance of the RPA estimated by the FS model is defined by R_{F} (km), the RPA is calculated as a circle centered on the BS with a radius R_{F}. Because $L(P_{\text{th}})$ is equal to $L_{\text{F}}(d = R_{\text{F}})$, R_{F} can be obtained as follows:

$$R_{\text{F}} = 10^{\alpha/20} \tag{3}$$

$$\alpha = P_{\text{t}} + G_{\text{t}} + G_{\text{r}} - P_{\text{th}} - 32.44 - 20\log_{10} f. \tag{4}$$

Because the FS model is an ideal physical model in free space and does not consider any diffraction or reflection due to terrain or buildings, it vastly over estimates the RPA which reduces the spatial-spectral efficiency [32].

B. EXTENDED-HATA MODEL (EH MODEL)

The EH model is an empirical radio propagation loss model [28]. Therefore, the formulas differ between the urban and suburban areas. The EH models for the urban and suburban area are called as the *EHU model* and *EHS model*, respectively. The propagation losses calculated using the EHU model, $L_{\text{U}}(d)$ (dB), and the EHS model, $L_{\text{S}}(d)$ (dB), are described as follows:

$$L_{\text{U}}\left(d\right) = v + w\log_{10}\left(d\right) \tag{5}$$

$$L_{\text{S}}\left(d\right) = L_{\text{U}}\left(d\right) - c - 5.4 \tag{6}$$

$$\begin{aligned} v = {} & 69.6 + 26.2\log_{10}\left(f\right) \\ & - 13.82\log_{10}\left(\max\left\{30, H_{\text{b}}\right\}\right) - a - b, \end{aligned} \tag{7}$$

$$w = 44.9 - 6.55\log_{10}\left(\max\left\{30, H_{\text{b}}\right\}\right) \tag{8}$$

$$\begin{aligned} a = {} & \left(1.1\log_{10}\left(f\right) - 0.7\right)\min\left\{10, H_{\text{m}}\right\} \\ & - \left(1.56\log_{10}\left(f\right) - 0.8\right) \\ & + \max\left\{020\log_{10}\left(\frac{H_{\text{m}}}{10}\right)\right\} \end{aligned} \tag{9}$$

$$b = \min\left\{020\log_{10}\left(\frac{H_{\text{b}}}{30}\right)\right\} \tag{10}$$

$$c = 2\left\{\log_{10}\left[\frac{\min\left\{\max\left\{150, f\right\}, 2000\right\}}{28}\right]\right\}^2 \tag{11}$$

$$H_{\text{m}} = \min\left\{h_{\text{b}}, h_{\text{m}}\right\} \tag{12}$$

$$H_{\text{b}} = \max\left\{h_{\text{b}}, h_{\text{m}}\right\} \tag{13}$$

where h_{b} and h_{m} are the antenna heights of the BS and MS, respectively. The applicable range of each parameter is 150 MHz $< f \leq$ 1500 MHz, 0.1 km $< d \leq$ 20 km, $h_{\text{b}} \leq$ 200 m, and $h_{\text{m}} \leq$ 200 m, respectively. Similar to the FS model, when the received power threshold for determining the RPA is P_{th}, the RPA calculated using the EHU or EHS model becomes a circle centered on the BS with radius R_{U} (km) or radius R_{S} (km). Because $L(P_{\text{th}})$ equals $L_{\text{U}}(d = R_{\text{U}})$ and $L_{\text{S}}(d = R_{\text{S}})$, R_{U} and R_{S} are calculated as follows:

$$R_{\text{U}} = 10^{(v - L(P_{\text{th}}))/(-w)} \tag{14}$$

$$R_{\text{S}} = 10^{(v - c - 5.4 - L(P_{\text{th}}))/(-w)} \tag{15}$$

Because the EH model is developed based on extensive experimental results, it represents the average characteristics of propagation loss. The actual propagation loss can be above or below this average. Therefore, the RPA estimated using the EH model results in excessive or insufficient protection. From the viewpoint of interference avoidance, insufficient protection in particular is problematic when used for RPA estimation [32], [33], [34]. Therefore, a large distance margin must be added to fully protect the primary user. However, this would result in excessive protection, even in areas that do not require protection, resulting in degradation of the spatial-spectral efficiency [32].

TABLE 1. ARIB STD-T103-compliant Experimental Instruments Parameters

Parameters	Values
Air interface	ARIB STD-T103 (Mode 1) [2]
Center frequency	195 MHz
Channel bandwidth	5 MHz
Modulation method	QPSK
Access method	OFDMA/TDD
FFT sampling frequency	5.6 MHz
Occupied bandwidth	4.9 MHz
FFT size	1,024
Subcarrier spacing	5.47 kHz
Frame length	10 ms
CP length / OFDM symbol length	1/8
Tx power	5 W (37 dBm)
BS antenna	Omni-directional ground-plane antenna (Gain: 2.15 dBi)
MS antenna	Omni-directional whip antenna (Gain: 2.15 dBi)
BS antenna height	Urban area: 20 m Suburban area: 18 m
MS antenna height	2.0 m (On rooftop of vehicle)

III. PERFORMANCE CONFIRMATION OF CONVENTIONAL MODELS USING ACTUAL VHF-BAND EXPERIMENT

In this section, we validated the RPA estimation performance of the conventional models by using actual VHF-band propagation measurement data in urban and suburban experimental fields to highlight the problems with the conventional models and to clarify the motivation for this paper.

A. EXPERIMENTAL INSTRUMENTS

The ARIB STD-T103-compliant BS and MS [5] were used in the VHF-band radio propagation measurement experiments in each field. The ARIB STD-T103 transmission signal is based on orthogonal frequency division multiplexing (OFDM). The propagation measurements can be performed using 840 subcarriers in a 5 MHz bandwidth [2], allowing the averaging of multipath fading and other effects. The setup parameters of the BS and MS are listed in Table 1.

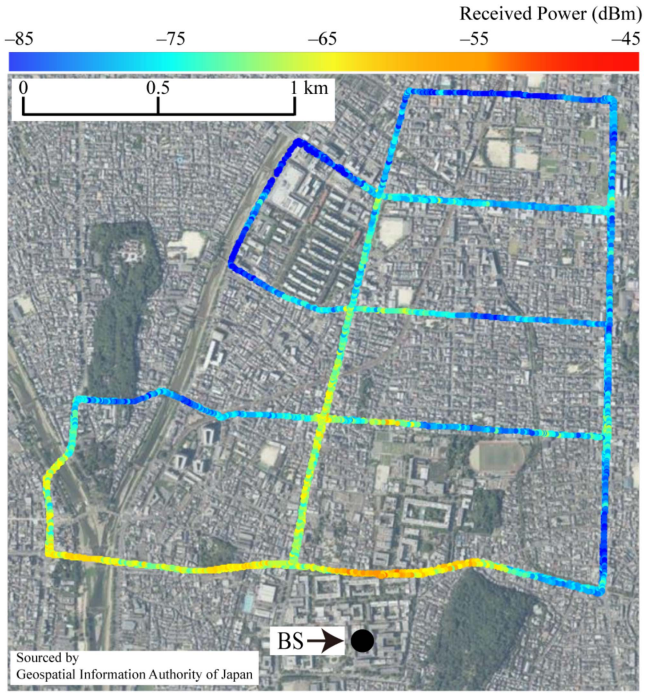

FIGURE 1. Experimental field for measurements in an urban area (Sakyo-ku, Kyoto, Japan) and received power measured at each location.

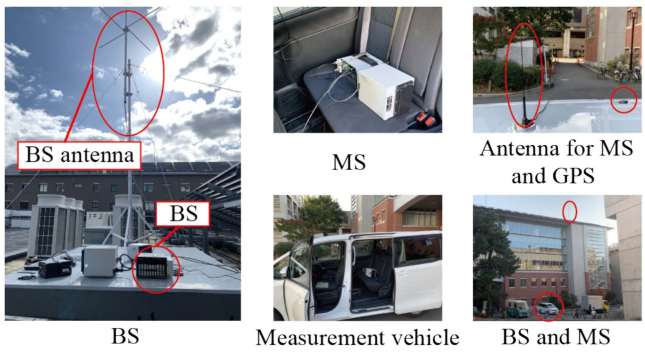

FIGURE 2. BS and MS installations of the experiment conducted in an urban area.

As described in Section I, this study aims to propose an RPA estimation model for the realization of highly efficient spectrum sharing in the V-High-band (207.5–222 MHz). However, it is not possible to emit radio waves in the V-High band at this time because specific legislation has not yet been passed. Therefore, this experiment was conducted in the 195 MHz band with 5 MHz channel bandwidth, which is very close to the target band and for which we have been granted an experimental license by the Japanese government.

B. EXPERIMENT CONDUCTED IN AN URBAN AREA

1) MEASUREMENT FIELD AND INSTRUMENTAL SETUP

The urban area shown in Fig. 1(Sakyo, Kyoto, Japan) was selected as the experimental field for the urban area measurements. As shown in Fig. 2, the BS was installed on the roof of the International Science Innovation Building at Kyoto University. The BS antenna (horizontal omnidirectional ground-plane antenna with 2.15 dBi gain) was mounted on top of the building (20 m above the ground level). The MS was installed in a measurement vehicle with the MS antenna (horizontal omnidirectional whip antenna with 2.15 dBi gain) and GPS antenna mounted on the vehicle's roof (2.0 m above the ground level).

The MS on the measurement vehicle received the ARIB STD-T103 downlink signal at the measurement location and measured its received power and GPS information per second. Measurements were performed while moving at an average speed of approximately 22 km/h (maximum speed of approximately 50 km/h). We conducted four rounds of the measurement route on the north side of the main campus of Kyoto University, as shown in Fig. 1, and obtained data for 14252 points.

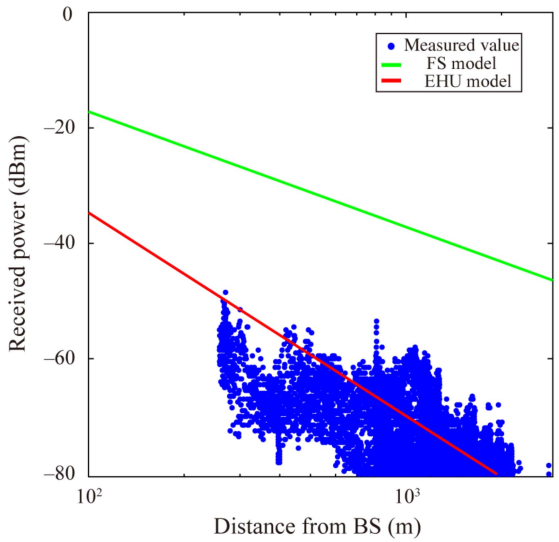

FIGURE 3. Relationship between the distance from transmitter to the receiver and received power based on the experimental results, FS model, and EHU model.

2) MEASUREMENT RESULTS AND RPA ESTIMATION PERFORMANCE OF CONVENTIONAL MODELS

The measured received power, P_M, is illustrated using the heatmap in Fig. 1. Additionally, Fig. 3 shows the relationship between d (i.e., the distance from the BS (transmitter) and MS (receiver)) and the received power measured through the experiment and the relationship between d and the received power calculated using the FS and EHU models. As shown in Fig. 3, the received power calculated using the FS model is above the measured received power, and the received power calculated using the EHU model represents the average characteristics of the measured received power. These results suggest that the FS model estimates a much larger RPA than the actual RPA and the EHU model has the tendency to estimate an RPA smaller than the actual RPA or larger than the actual RPA, depending on the location.

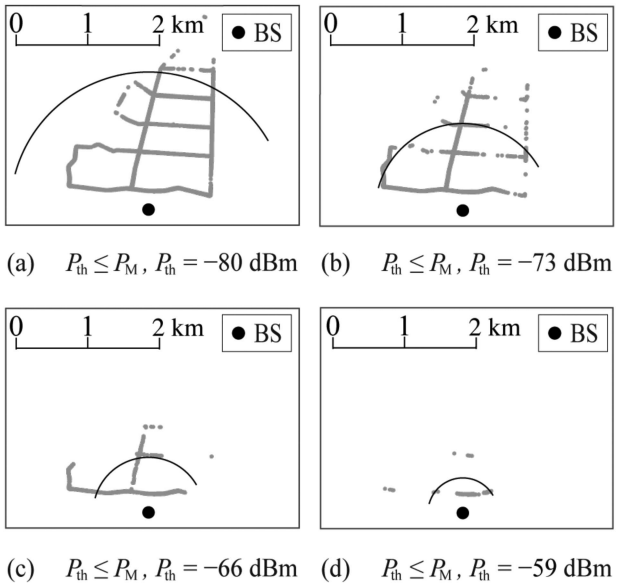

FIGURE 4. Measurement locations where the received power is above P_{th} dBm, obtained by the experiment in an urban area, and the boundary of the region where the received power is above P_{th} dBm estimated using the EHU model.

The results when plotting only the measurement locations with $P_M \ge P_{th}$ and the RPA based on the EHU model calculated using (14) with each P_{th} are shown in Fig. 4. In Fig. 4(a)–(d), P_{th} is set to –80, –73, –66, and –59 dBm, respectively. To completely avoid intersystem interference, all measurement locations with $P_M > P_{th}$ must exist inside the estimated RPA with P_{th}. However, as shown in Fig. 4, some measurement locations were outside the estimated RPA, thus preventing the EHU model from achieving perfect interference avoidance. Furthermore, the EHU model also sets up excessive RPAs in some locations, as shown in Fig. 4(a).

When the RPA is estimated using the FS model, the protection distance (the radius of the RPA) was calculated according to (3) as 142.1, 63.45, 28.34, and 12.66 km when P_{th} = –80 dBm, –73 dBm, –66 dBm, and –59 dBm, respectively. This shows that the RPAs are set excessively compared to the actual measured received power, as shown in Figs. 3 and 4.

C. EXPERIMENT CONDUCTED IN A SUBURBAN AREA

1) MEASUREMENT FIELD AND INSTRUMENTAL SETUP

The suburban area shown in Fig. 5(Seika, Soraku, Kyoto, Japan) was selected as the experimental field for suburban area measurements. As shown in Fig. 6, the BS was installed on the roof of the West Wing Building of the Advanced Telecommunications Research Institute International (ATR). The BS antenna (horizontal omnidirectional ground-plane antenna with 2.15 dBi gain) was mounted on the roof of the building (18 m above the ground level). The MS was installed in a measurement vehicle. The MS antenna (horizontal omnidirectional whip antenna with 2.15 dBi gain) and GPS antenna were mounted on the vehicle's roof (2.0 m above the ground level).

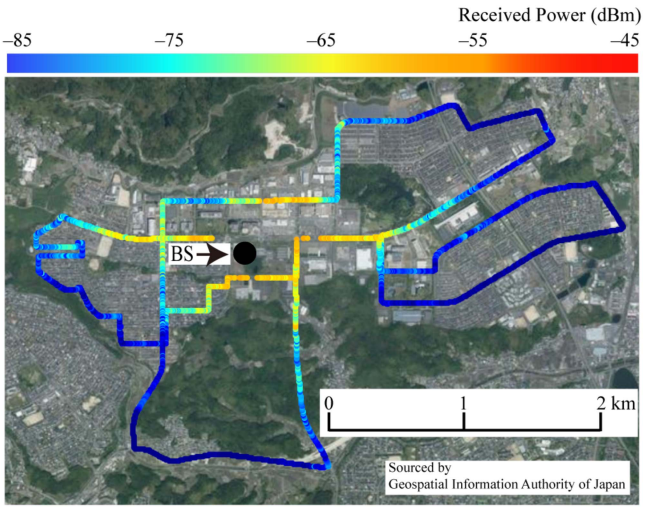

FIGURE 5. Experimental field for measurements in a suburban area (Seika, Soraku, Kyoto, Japan) and received power measured at each location.

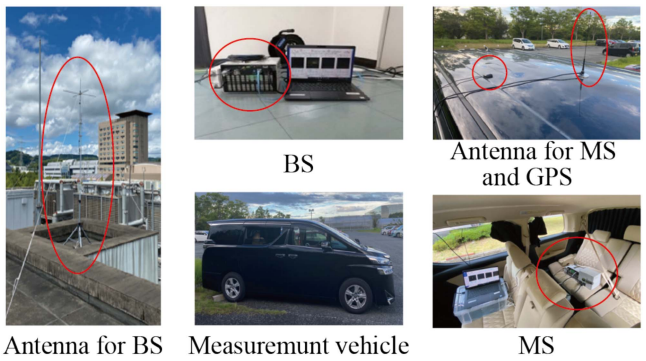

FIGURE 6. BS and MS installations of the experiment conducted in a suburban area.

The MS on the measurement vehicle received the ARIB STD-T103 downlink signal at the measurement location and measured its received power and GPS information every second. Measurements were performed while moving at an average speed of approximately 24 km/h (maximum speed of approximately 50 km/h). We performed four rounds of the measurement route, as shown in Fig. 5 and obtained data of 15781 points.

2) MEASUREMENT RESULTS AND RPA ESTIMATION PERFORMANCE OF CONVENTIONAL MODELS

The measured received power, P_M, is illustrated using the heatmap in Fig. 5. In addition, Fig. 7 shows the relationship between d and the received power measured through the experiment and the relationship between d and the received power calculated using the FS and EHS models. From the figure, we can confirm that the received power calculated using the FS model is above the measured received power, and the received power calculated using the EHU model represents the average characteristics of the measured received power, similar to the results in the urban areas.

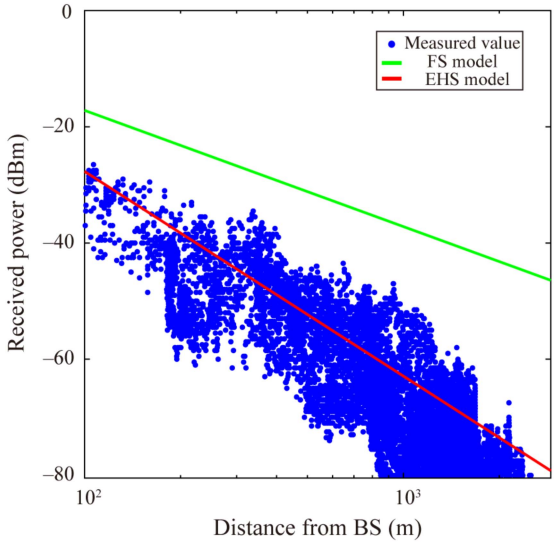

FIGURE 7. Relationship between the distance from transmitter to the receiver and received power based on the experimental results, FS model, and EHS model.

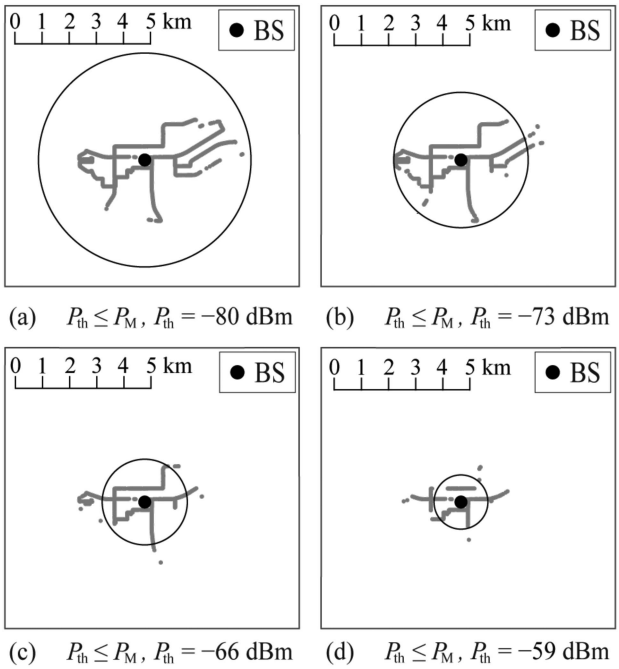

FIGURE 8. Measurement locations where the received power is above P_{th} dBm, obtained by the experiment in the suburban area, and the boundary of the region where the received power is above P_{th} dBm, estimated using the EHS model.

The results of plotting only the measurement locations with $P_M \ge P_{th}$ and the RPA based on the EHS model, calculated using (15), with each P_{th} are shown in Fig. 8. In Fig. 8(a)–(d), P_{th} is set to –80, –73, –66, and –59 dBm, respectively. As mentioned earlier, all measurement locations with $P_M > P_{th}$ must exist inside the estimated RPA with P_{th} to completely avoid intersystem interference. However, as shown in Fig. 8, some measurement locations were outside the estimated RPA, thus

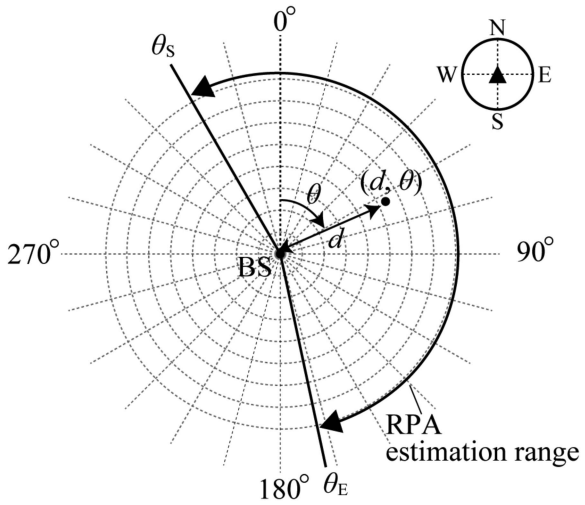

FIGURE 9. Counterclockwise polar coordinate system for RPA estimation.

preventing the EHS model from achieving perfect interference avoidance. Furthermore, the EHS model also sets up excessive RPAs in some locations, as shown in Fig. 8(a).

When the RPA is estimated using the FS model, the protection distance (i.e., the radius of the RPA) can be calculated according to (3) as 142.1 km, 63.45 km, 28.34 km, and 12.66 km when $P_{th} = -80$, –73, –66, and –59 dBm, respectively. This indicates that the RPAs are set excessively compared to the actual measured received power (Fig. 8).

IV. PROPOSED MODEL FOR RPA ESTIMATION

We propose an effective RPA estimation model that achieves full protection and avoids overprotection by adding location gain to the EH model. First, we defined the location gain and described the basic concept of the proposed model. Subsequently, we developed a location-gain estimation formula using topographic data.

Prior to the proposal, we defined the coordinate system for RPA estimation. The location (d, θ) is defined by the measurement point in a clockwise polar coordinate system, as shown in Fig. 9. The origin is the BS to be protected and the starting line is the direction of true north. θ ($\theta_S \le \theta < \theta_E$) indicates the azimuth angle, and θ_S and θ_E indicate the ranges to be calculated. For example, if the RPA is calculated for all directions with the BS as the origin, θ_S and θ_E are set as 0° and 360°, respectively.

A. MODEL CONCEPT AND DEFINITION OF THE LOCATION GAIN

The proposed model aims to achieve an efficient RPA estimation that combines *full protection* and *reduction of the overprotected area* by adding a location-specific correction value (that is, location gain) to the RPA estimated using the EH model. The location gain, $G(d, \theta)$ (dB), at location (d, θ) is defined as the difference between the actual received power $P(d, \theta)$ (dBm) and the estimated received power $P_E(d)$ (dBm)

calculated using the EH model as follows:

$$G(d,\theta) = P(d,\theta) - P_{\mathrm{E}}(d) \tag{16}$$

$$P_{\mathrm{E}}(d) = P_{\mathrm{t}} + G_{\mathrm{t}} + G_{\mathrm{r}} - L_{\mathrm{E}}(d) \tag{17}$$

where $L_{\mathrm{E}}(d)$ is the propagation loss calculated using the EH model at location (d, θ). If the target field is an urban area or a suburban area, $L_{\mathrm{E}}(d)$ can be calculated as $L_{\mathrm{E}}(d) = L_{\mathrm{U}}(d)$ or $L_{\mathrm{E}}(d) = L_{\mathrm{S}}(d)$, respectively.

Since the location gain is present at each arbitrary point, we essentially need to calculate the individual location gains for all the locations. Because the number of locations is infinite, the computational complexity becomes large. Therefore, the target field was divided into several regions according to the angle, and the protection distance was calculated for each region. By limiting the number of regions for calculating the location gain to a finite number, the amount of calculation is reduced. Assume that N is the number of divisions and any location $(d^{(n)}, \theta^{(n)})$ included in the n-th region satisfies the following:

$$d^{(n)} \geq 0 \tag{18}$$

$$\theta_{\mathrm{S}} + \frac{(n-1)(\theta_{\mathrm{E}} - \theta_{\mathrm{S}})}{N} \leq \theta^{(n)} < \theta_{\mathrm{S}} + \frac{n(\theta_{\mathrm{E}} - \theta_{\mathrm{S}})}{N} \tag{19}$$

where n is an integer of $0 < n \leq N$. Assume that $G(d^{(n)}, \theta^{(n)})$ is the location gain at a point included in the n-th region. Thus, its maximum value, $G^{(n)}$, is defined as the *representative location gain* of the n-th region as follows:

$$G^{(n)} = G\left(d_{\mathrm{R}}^{(n)}, \theta_{\mathrm{R}}^{(n)}\right) = \max\left\{G\left(d^{(n)}, \theta^{(n)}\right)\right\} \tag{20}$$

The location $(d_{\mathrm{R}}^{(n)}, \theta_{\mathrm{R}}^{(n)})$ at which the representative location gain is obtained is called the *representative location* of the n-th region. Using the calculated $G^{(n)}$, the protection distance for the n-th region in the urban area $R_{\mathrm{PU}}^{(n)}$ and in the suburban area $R_{\mathrm{PS}}^{(n)}$ can be calculated as follows:

$$R_{\mathrm{PU}}^{(n)} = 10^{\left\{\left(v - L^{(n)}(P_{\mathrm{th}})\right)/(-w)\right\}} \tag{21}$$

$$R_{\mathrm{PS}}^{(n)} = 10^{\left\{\left(v - c - 5.4 - L^{(n)}(P_{\mathrm{th}})\right)/(-w)\right\}} \tag{22}$$

$$L^{(n)}(P_{\mathrm{th}}) = P_{\mathrm{t}} + G_{\mathrm{t}} + G_{\mathrm{r}} + G^{(n)} - P_{\mathrm{th}} \tag{23}$$

Using the representative location gain, which is the maximum location gain in the n-th region, full protection in the n-th region should be achieved.

Fig. 10 shows an example of the RPA estimated using the proposed model in an urban area. In this example, the RPA estimation range is divided into $N = 7$. When $G^{(n)} > 0$, the physical meaning of $G^{(n)}$ is a positive margin to expand the RPA, estimated using the EH model, for preventing the generation of unprotected areas, as shown in the 6th region in Fig. 9. When $G^{(n)} < 0$, the physical meaning of $G^{(n)}$ is the negative margin to reduce the RPA, estimated using the EH model, for preventing the generation of overprotected areas, as shown in the 7th region in Fig. 9.

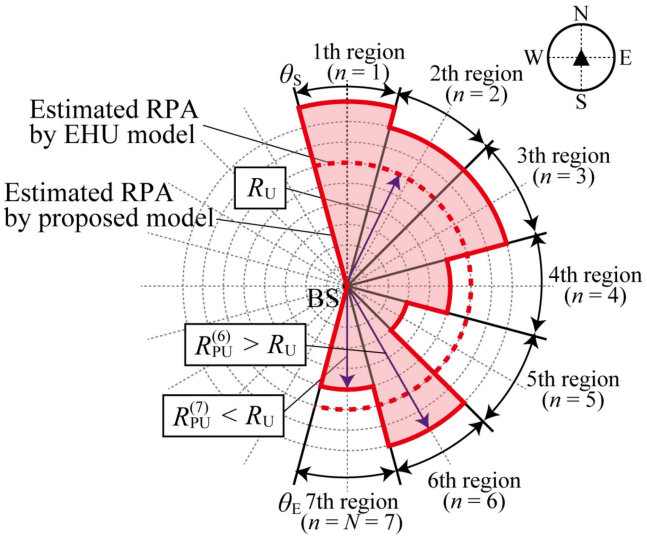

FIGURE 10. Example of RPA estimated using the proposed model in an urban area.

B. ESTIMATION OF THE LOCATION GAIN

To calculate the proposed RPA, $R_{\mathrm{PU}}^{(n)}$ or $R_{\mathrm{PS}}^{(n)}$, we must obtain the actual received power $P(d, \theta)$ in (16). However, the measurement of all the $P(d, \theta)$ values at every point in the target field is unrealistic. Therefore, we developed an equation that can estimate $G^{(n)}$ in (20) using terrain profiles.

First, assuming that the location gain depends on the distance and diffraction losses, we developed an estimation formula for $G(d, \theta)$ as follows:

$$G_{\mathrm{E}}(d,\theta) = k_1 \log_{10} d + k_2 J(d,\theta) + C \tag{24}$$

where $G_{\mathrm{E}}(d, \theta)$ denotes the estimated $G(d, \theta)$, and $J(d, \theta)$ is the diffraction loss calculated using the Bullington model—single-point knife-edge diffraction model [35] with terrain and building information. k_1, k_2, and C indicate the adjustment coefficients to be designed using the results of the actual radio propagation experiments presented in Section III.

The location gain calculated from the measured received power at the location of $(d^{(n)}, \theta^{(n)})$ in the n-th region, $G_{\mathrm{M}}(d^{(n)}, \theta^{(n)})$, is expressed using (16) as follows:

$$G_{\mathrm{M}}\left(d^{(n)}, \theta^{(n)}\right) = P_{\mathrm{M}}\left(d^{(n)}, \theta^{(n)}\right) - P_{\mathrm{E}}\left(d^{(n)}\right) \tag{25}$$

where $P_{\mathrm{M}}(d^{(n)}, \theta^{(n)})$ is the measured received power from the experiment and includes the effect of shadowing, blockage obstacles, and reflection obstacles, as it is the actual experimental result. Here, $P_{\mathrm{E}}(d^{(n)})$ also includes the effect of shadowing, blockage obstacles, and reflection obstacles because the EH model is developed on the basis of the extensive experimental results. Thus, $G_{\mathrm{M}}(d^{(n)}, \theta^{(n)})$ includes the combination all of the aforementioned effects.

The representative location gain of the n-th region, $G_{\mathrm{M}}^{(n)}$, can be calculated using (20) as follows:

$$G_{\mathrm{M}}^{(n)} = G_{\mathrm{M}}\left(d_{\mathrm{R}}^{(n)}, \theta_{\mathrm{R}}^{(n)}\right) = \max\left\{G_{\mathrm{M}}\left(d^{(n)}, \theta^{(n)}\right)\right\}. \tag{26}$$

Using the terrain and building information between the representative and the BS locations in each region, the diffraction loss can be determined using the Bullington model to include the effect of diffraction. Because the objective is to obtain $G_{\mathrm{E}}(d_{\mathrm{R}}^{(n)}, \theta_{\mathrm{R}}^{(n)}) = G_{\mathrm{M}}(d_{\mathrm{R}}^{(n)}, \theta_{\mathrm{R}}^{(n)})$, the following equation must hold from (24) and (26):

$$G_{\mathrm{M}}^{(n)} = k_1 \log_{10} d_{\mathrm{R}}^{(n)} + k_2 J\left(d_{\mathrm{R}}^{(n)}, \theta_{\mathrm{R}}^{(n)}\right) + C \tag{27}$$

where $G_{\mathrm{M}}^{(n)}$, $d_{\mathrm{R}}^{(n)}$, and $J(d_{\mathrm{R}}^{(n)}, \theta_{\mathrm{R}}^{(n)})$ are known. Thus, we have N relational equations to determine the three undetermined coefficients—k_1, k_2, and C. In this study, we propose two methods to resolve this problem: determining using three simultaneous equations and multiple regression analysis.

1) METHOD-A: THREE SIMULTANEOUS EQUATIONS

Because of three undetermined coefficients, we need three simultaneous equations to obtain the solution. Therefore, three equations should be selected to obtain the solution from N equations. In the proposed method, $n = n_1$ for the maximum $G_{\mathrm{M}}^{(n)}$, $n = n_2$ for the maximum $d_{\mathrm{R}}^{(n)}$, and $n = n_3$ for the maximum $J\left(d_{\mathrm{R}}^{(n)}, \theta_{\mathrm{R}}^{(n)}\right)$ are selected, and the coefficients are determined by solving the simultaneous equations shown in (27).

2) METHOD-B: MULTIPLE REGRESSION ANALYSIS

In this method, the three coefficients are determined by performing a multiple regression analysis based on the least-squares method using all N equations. The coefficients are determined as values that minimize the sum of squares of the difference between the measured and estimated location gains.

$$\Delta G^{(n)}(k_1, k_2, C) = G_{\mathrm{M}}^{(n)} - G_{\mathrm{E}}^{(n)} \tag{28}$$

$$\{k_1, k_2, C\} = \underset{k_1, k_2, C}{\arg\min} \sum_{n=1}^{N} \left|\Delta G^{(n)}(k_1, k_2, C)\right|^2 \tag{29}$$

where $G_{\mathrm{E}}^{(n)} = G_{\mathrm{E}}(d_{\mathrm{R}}^{(n)}, \theta_{\mathrm{R}}^{(n)})$. The variance inflation factor value v, is an indicator of multicollinearity. If $v \leq 5$, a statistically reliable regression equation without multicollinearity is considered to have been obtained [36]. This method is referred to in this study as *Method-B*.

Using Method-A or -B, the coefficients k_1, k_2, and C can be determined and the estimated location gain $G_{\mathrm{E}}^{(n)}$ can be obtained. When $G_{\mathrm{E}}^{(n)} < G_{\mathrm{M}}^{(n)}$, the coefficient C is updated as $C' = C + G_{\mathrm{C}}$ to prevent the generation of unprotected areas, where G_{C} is the adjustment value calculated as

$$G_{\mathrm{C}} = \max\left\{g_{\mathrm{C}}^{(n)}\right\} \tag{30}$$

$$g_{\mathrm{C}}^{(n)} = \max\left\{0, G_{\mathrm{M}}^{(n)} - G_{\mathrm{E}}^{(n)}\right\} \tag{31}$$

Finally, the estimated location gain for the n-th region is obtained as follows:

$$G_{\mathrm{E}}^{(n)} = k_1 \log_{10} d^{(n)} + k_2 J\left(d^{(n)}, \theta^{(n)}\right) + C' \tag{32}$$

TABLE 2. Experimental Data to Determine the Coefficients of the Estimation Formula of the Location Gain in an Urban Area

n	$G_{\mathrm{M}}^{(n)}$ (dB)	$d_{\mathrm{R}}^{(n)}$ (km)	$J\left(d_{\mathrm{R}}^{(n)}, \theta_{\mathrm{R}}^{(n)}\right)$ (dB)
1	12.9857	1.1448	11.6453
2	11.4592	1.2605	8.0988
3	2.1363	1.1561	24.1874
4	0.2459	0.8677	31.8919
5	9.2557	0.8403	21.7305
6	13.1497	0.8077	13.9824
7	12.1714	1.9548	16.5898
8	11.0527	1.8170	16.8097
9	6.9787	1.1823	23.7255

V. PROPOSED MODEL EVALUATION BY MEASUREMENT EXPERIMENTS IN AN URBAN AREA

This section evaluates the proposed RPA estimation method in an urban area using the experimental results described in Section III. First, the coefficients in the location-gain estimation formula (32) were determined using the measurement results of the experiment conducted in the urban area. Subsequently, the RPA estimation performance of the proposed model was evaluated.

A. ESTIMATION OF THE LOCATION GAIN

1) EXPERIMENTAL DATA TO DETERMINE THE COEFFICIENTS OF THE LOCATION GAIN ESTIMATION FORMULA

The measurement data of the received power, shown in Fig. 1, were used in this evaluation. θ_{S}, θ_{E}, and N were set as $\theta_{\mathrm{S}} = -75^\circ$, $\theta_{\mathrm{E}} = 60^\circ$, and $N = 9$, respectively. Table 2 shows $G_{\mathrm{M}}^{(n)}$, $d_{\mathrm{R}}^{(n)}$, and $\left(d_{\mathrm{R}}^{(n)}, \theta_{\mathrm{R}}^{(n)}\right)$ obtained from the measurement data in the experiment.

2) LOCATION GAIN ESTIMATION USING METHOD-A

From Table 2, we selected three measurement datasets: $n_1 = 6$, $n_2 = 7$, and $n_3 = 4$. Therefore, coefficients k_1, k_2, and C were determined using the following equations:

$$G_{\mathrm{M}}^{(6)} = k_1 \log_{10} d_{\mathrm{R}}^{(6)} + k_2 J\left(d_{\mathrm{R}}^{(6)}, \theta_{\mathrm{R}}^{(6)}\right) + C \tag{33}$$

$$G_{\mathrm{M}}^{(7)} = k_1 \log_{10} d_{\mathrm{R}}^{(7)} + k_2 J\left(d_{\mathrm{R}}^{(7)}, \theta_{\mathrm{R}}^{(7)}\right) + C \tag{34}$$

$$G_{\mathrm{M}}^{(4)} = k_1 \log_{10} d_{\mathrm{R}}^{(4)} + k_2 J\left(d_{\mathrm{R}}^{(4)}, \theta_{\mathrm{R}}^{(4)}\right) + C. \tag{35}$$

By solving the simultaneous Equations (33)–(35), $k_1 = 2.3735$, $k_2 = -0.7246$, and $C = 23.5018$ were obtained. Thus, the location gains in each region are estimated as follows:

$$G_{\mathrm{E}}^{(n)} = k_1 \log_{10} d_{\mathrm{R}}^{(n)} + k_2 J\left(d_{\mathrm{R}}^{(n)}, \theta_{\mathrm{R}}^{(n)}\right) + C. \tag{36}$$

Fig. 11(a) shows the relationship between $G_{\mathrm{M}}^{(n)}$ and $G_{\mathrm{E}}^{(n)}$ estimated using (36) with $k_1 = 2.3735$, $k_2 = -0.7246$, and $C = 23.5018$. $G_{\mathrm{C}} = 1.6797$ was obtained from Fig. 11(a), and C was updated to $C' = 25.1815$. Fig. 11(b) shows the relationship between $G_{\mathrm{M}}^{(n)}$ and $G_{\mathrm{E}}^{(n)}$ estimated using (36) with

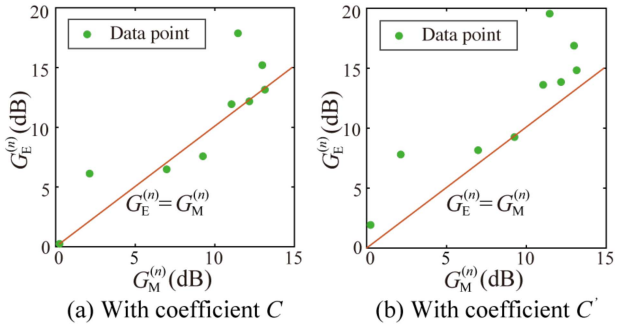

FIGURE 11. Relationship between $G_M^{(n)}$ and $G_E^{(n)}$ estimated using Method-A.

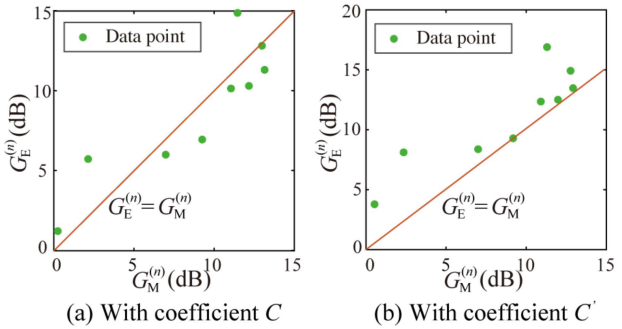

FIGURE 12. Relationship between $G_M^{(n)}$ and $G_E^{(n)}$ estimated using Method-B.

$k_1 = 2.3735$, $k_2 = -0.7246$, and $C' = 25.1815$. We validated that $G_M^{(n)} \leq G_E^{(n)}$ was achieved in all the regions.

3) LOCATION GAIN ESTIMATION USING METHOD-B

Using the measurement datasets shown in Table 2 and (24), (28), and (29), we obtain $k_1 = 1.2230$, $k_2 = -0.5655$, and $C = 19.3407$. This multiple regression analysis has a value of $v = 1.107 \leq 5$ and is a statistically reliable regression equation without multicollinearity. Fig. 12(a) shows the relationship between $G_M^{(n)}$ and $G_E^{(n)}$ estimated using (36) with $k_1 = 1.2230$, $k_2 = -0.5655$, and $C = 19.3407$. $G_C = 2.2968$ is obtained from Fig. 12(a), and C is updated using $C' = 21.6375$. Fig. 12(b) shows the relationship between $G_M^{(n)}$ and $G_E^{(n)}$ estimated using (36) with $k_1 = 1.2230$, $k_2 = -0.5655$, and $C' = 21.6375$. We validated that $G_M^{(n)} \leq G_E^{(n)}$ is achieved in all the regions.

B. EVALUATION OF THE PROPOSED MODEL

We evaluated the RPA estimation performance of the proposed models using Methods-A and -B. As earlier mentioned, the estimated RPA must be as small as possible to avoid generating unprotected areas. As mentioned in Section III, the EHU model cannot achieve perfect interference avoidance. Therefore, the proposed model was compared with the FS model and the *fixed location-gain model* in which the maximum location gain obtained from the measurements (i.e., $G_M^{(6)} = 13.1497$ dB) is applied to all regions.

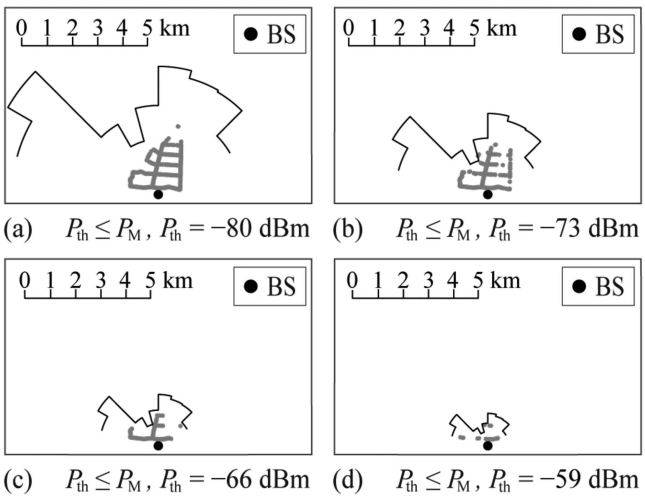

FIGURE 13. RPA estimated using the proposed model with Method-A in the urban area.

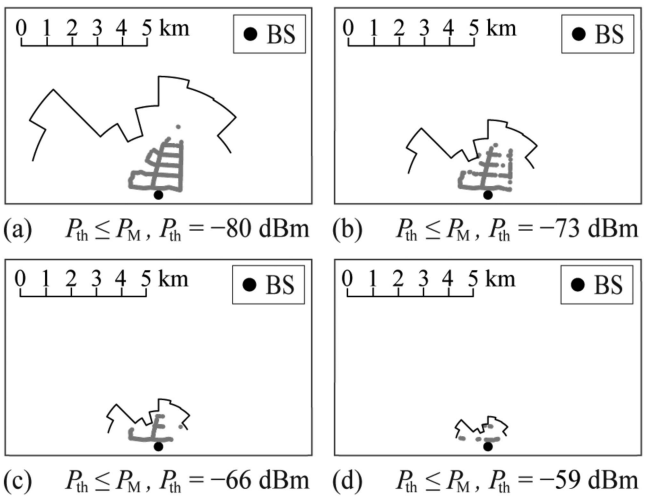

FIGURE 14. RPA estimated using the proposed model with Method B in urban area.

Figs. 13, 14, and 15 show the RPA estimated by the proposed models using Method-A, Method-B, and the fixed location gain, respectively, along with the results of plotting only the measurement locations with $P_{th} \leq P_M$. Based on these visualization results, the RPAs estimated using all three methods encompass the actual values and achieve 100% radio protection.

Table 3 shows the size of the RPA estimated by the FS model, the fixed location gain model, and the proposed model using Method-A and Method-B. Regardless of the P_{th}, the models were employed in increasing order of RPA size: the proposed model using Method-B, the proposed model with Method-A, the fixed location gain model, and the FS model, respectively. When $P_{th} = -80$ dBm, the proposed model using Method-B can reduce the RPA size by 2.375×10^4 km^2 (99.92%), 44.15 km^2 (67.40%), and

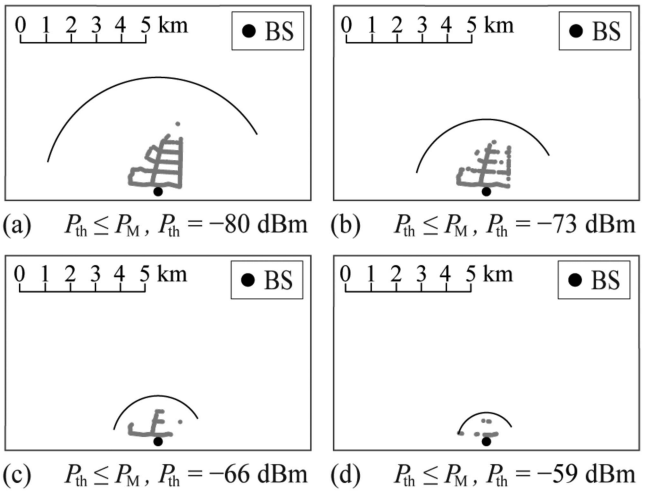

FIGURE 15. RPA estimated using the fixed location-gain model in the urban area.

TABLE 3. RPA Size Comparison in an Urban Area

P_{th} (dBm)	FS model	Fixed location-gain model	Proposed model with Method-A	Proposed model with Method-B
−59	1.888×10^{2}	4.794	1.836	1.563
−66	9.461×10^{2}	1.364×10^{1}	5.226	4.448
−73	4.743×10^{3}	3.883×10^{1}	1.487×10^{1}	1.226×10^{1}
−80	2.377×10^{4}	6.550×10^{1}	2.509×10^{1}	2.135×10^{1}

3.74 km^2 (14.89%) compared to the FS model, fixed location gain model, and proposed model using Method-A, respectively.

VI. PROPOSED MODEL EVALUATION USING THE MEASUREMENT EXPERIMENTS IN A SUBURBAN AREA

This section evaluates the proposed RPA estimation method in a suburban area using the experimental measurement results described in Section III. First, the coefficients in the location gain estimation formula (32) were determined using the measurement results of the experiment conducted in the suburban area. Subsequently, the RPA estimation performance of the proposed model was evaluated.

A. ESTIMATION OF THE LOCATION GAIN

1) EXPERIMENTAL DATA TO DETERMINE THE COEFFICIENTS OF LOCATION GAIN ESTIMATION FORMULA

The measurement data of the received power, shown in Fig. 5, were used in this evaluation. θ_S, θ_E, and N were set as $\theta_S = 0^\circ$, $\theta_E = 360^\circ$, and $N = 18$, respectively. Table 4 lists $G_M^{(n)}$, $d_R^{(n)}$, and $(d_R^{(n)}, \theta_R^{(n)})$ obtained from the measurement data in the experiment.

2) ESTIMATION OF THE LOCATION GAIN USING METHOD-A

From Table 4, we selected three measurement datasets: $n_1 = 14$, $n_2 = 3$, and $n_3 = 17$. Therefore, coefficients k_1, k_2, and C

TABLE 4. Experimental Data for Determining of Location-gain Estimation Formula Coefficients in a Suburban Area

n	$G_M^{(n)}$ (dB)	$d_R^{(n)}$ (km)	$J\left(d_R^{(n)}, \theta_R^{(n)}\right)$ (dB)
1	3.6878	0.3523	6.3440
2	8.4292	1.0187	0.3013
3	5.6866	1.2604	16.1611
4	9.0179	1.0938	1.1317
5	13.3711	0.7816	−1.2515
6	−3.5156	0.7871	14.0628
7	−0.5045	0.2679	8.6008
8	1.4191	0.4880	0.1697
9	9.1814	0.5750	1.0297
10	−5.1728	0.2040	−0.0731
11	−1.4918	0.2595	−1.0232
12	7.7947	0.4920	0.0329
13	3.6440	0.7954	10.2645
14	16.5575	0.9313	6.6361
15	8.0017	0.7880	−1.3094
16	−1.2912	0.4583	−1.2086
17	−0.5110	0.4517	18.6363
18	3.4513	0.3469	0.3075

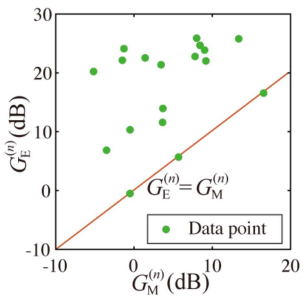

FIGURE 16. Relationship between $G_M^{(n)}$ and $G_E^{(n)}$ estimated by Method-A.

were determined using the following equations:

$$G_M^{(14)} = k_1 \log_{10} d_R^{(14)} + k_2 J\left(d_R^{(14)}, \theta_R^{(14)}\right) + C \tag{37}$$

$$G_M^{(3)} = k_1 \log_{10} d_R^{(3)} + k_2 J\left(d_R^{(3)}, \theta_R^{(3)}\right) + C \tag{38}$$

$$G_M^{(17)} = k_1 \log_{10} d_R^{(17)} + k_2 J\left(d_R^{(17)}, \theta_R^{(17)}\right) + C. \tag{39}$$

By solving the simultaneous equations (37)–(39), we obtain $k_1 = 5.9641$, $k_2 = -1.2236$, and $C = 24.8617$. Thus, the location gain in each region was estimated using (36).

Fig. 16 shows the relationship between $G_M^{(n)}$ and $G_E^{(n)}$ estimated using (36) with $k_1 = 5.9641$, $k_2 = -1.2236$, and $C = 24.8617$. Because $G_M^{(n)} \le G_E^{(n)}$ in all regions in Fig. 16, $G_C = 0$ and $C' = C$.

3) ESTIMATION OF THE LOCATION GAIN USING METHOD-B

Using the measurement datasets shown in Table 4 and (24), (28), and (29), we obtain $k_1 = 18.4882$, $k_2 = -0.3392$, and $C = 10.5400$. This multiple regression analysis has $v = 1.052 \le 5$ and is a statistically reliable regression equation without multicollinearity. Fig. 17(a) shows the relationship between

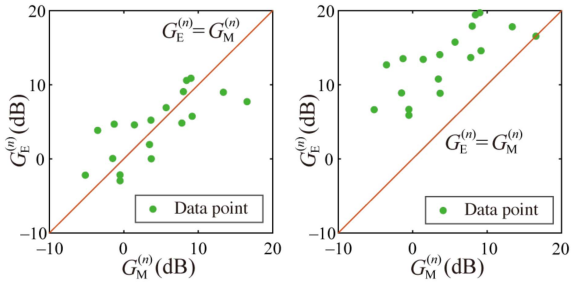

FIGURE 17. Relationship between $G_M^{(n)}$ and $G_E^{(n)}$ estimated by Method-B.

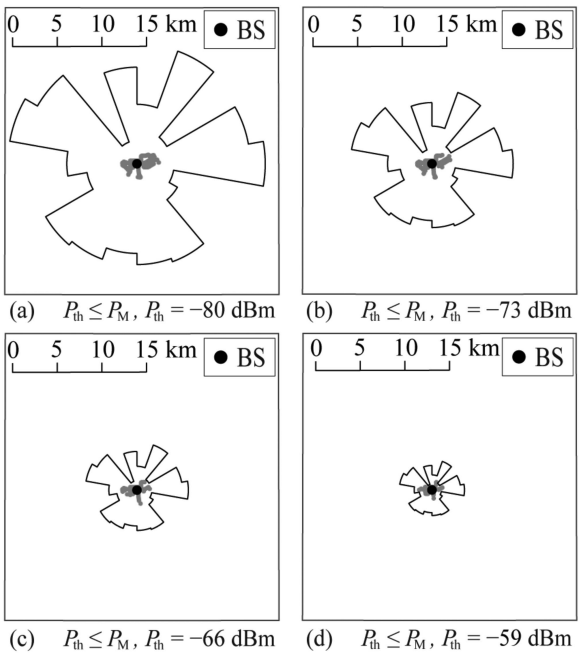

FIGURE 18. RPA estimated by the proposed model using Method-A in a suburban area.

$G_M^{(n)}$ and $G_E^{(n)}$ estimated using (36) with $k_1 = 18.4882$, $k_2 = -0.3392$, and $C = 10.5400$. From Fig. 17(a), $G_C = 8.8402$ was obtained and C was updated by $C' = 19.3802$. Fig. 17(b) shows the relationship between $G_M^{(n)}$ and $G_E^{(n)}$ estimated using (36) with $k_1 = 18.4882$, $k_2 = -0.3392$, and $C' = 19.3802$. We validated that $G_M^{(n)} \le G_E^{(n)}$ was achieved in all the regions.

B. EVALUATION OF THE PROPOSED MODEL

We evaluated the RPA estimation performance of the proposed models using Method-A and Method-B. As mentioned in Section III, the EHS model cannot achieve perfect interference avoidance. Therefore, the proposed model was compared with the FS model and the fixed location gain model in which the maximum measured location gain (that is, $G_M^{(14)} = 16.5575$ dB) is applied to all regions.

Figs. 18, 19, and 20 show the RPA estimated by the proposed models using Method-A, Method-B, and the fixed location gain, respectively, along with the results when plotting only the measurement locations with $P_{th} \le P_M$. Based on these visualization results, the RPAs estimated using all three methods encompass the actual values and achieve 100% radio protection.

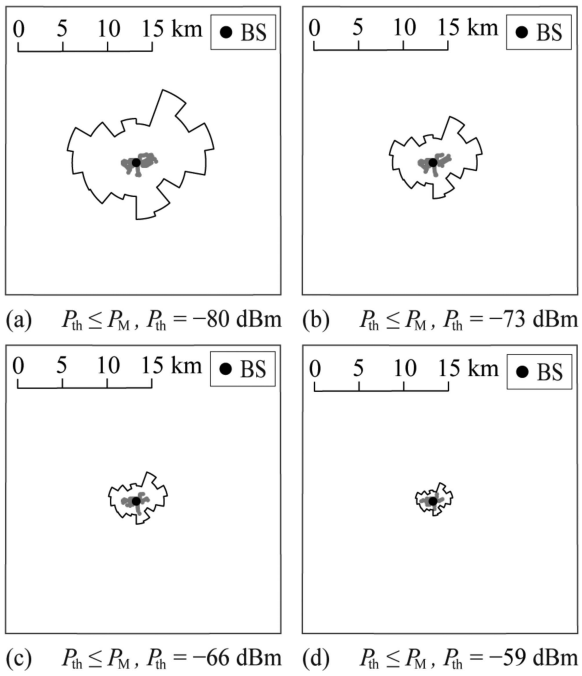

FIGURE 19. RPA estimated by the proposed model with Method-B in a suburban area.

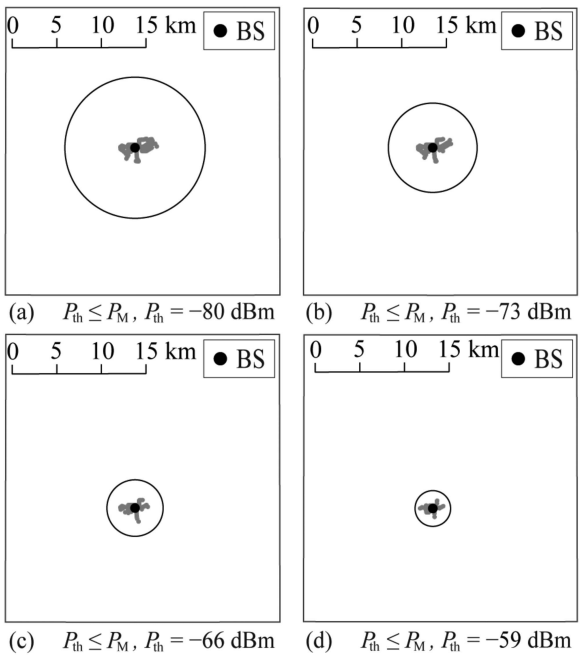

FIGURE 20. RPA estimated by the fixed location-gain model in a suburban area.

Table 5 shows the size of the RPA estimated by the FS model, fixed location gain model, and proposed models using Methods-A and -B. Regardless of P_{th}, the proposed model using Method-B can estimate the minimum RPA size.

TABLE 5. RPA Size Comparison in Suburban Area

P_{th} (dBm)	FS model	Fixed location-gain model	Proposed model with Method-A	Proposed model with Method-B
–59	5.035×10^{2}	4.794×10^{1}	2.220×10^{1}	9.710
–66	2.523×10^{3}	3.268×10^{1}	5.493×10^{1}	2.425×10^{1}
–73	1.265×10^{4}	8.161×10^{1}	1.372×10^{2}	6.055×10^{1}
–80	6.339×10^{4}	2.038×10^{2}	3.425×10^{2}	1.512×10^{2}

When $P_{th} = -80$ dBm, the proposed model using Method-B can reduce the RPA size by 6.323×10^5 km^2 (99.76%), 52.58 km^2 (34.78%), and 1.913×10^2 km^2 (54.83%) compared with the FS model, fixed location gain model, and proposed model using Method-A, respectively.

VII. CONCLUSION

This paper proposed an RPA estimation model that achieves full protection and avoids overprotection by adding an appropriate margin (i.e., location gain) to the EH model, for realizing efficient spectrum sharing in the V-High-band. This study experimentally obtained the location gain by conducting VHF-band propagation experiments in urban and suburban areas. Subsequently, an estimation formula for location gain, using topographic data, was developed. The developed estimation formula included correction terms based on experimental data. Therefore, propagation experiments to estimate the RPA using our developed RPA estimation formula are not necessary. In the urban area, when the threshold of the received power to determine the RPA is set to –80 dBm, the proposed model using Method-B reduced the RPA size by 99.92%, 67.40%, and 14.89% compared to the FS model, the fixed location gain model, and the proposed model using Method-A, respectively. In the suburban area, when the threshold of the received power to determine the RPA is set to –80 dBm, the proposed model with Method-B reduces the RPA size by 99.76%, 34.78%, and 54.83% compared to the FS model, fixed location gain model, and proposed model using Method-A, respectively. The proposed RPA estimation model can realize an efficient spectrum sharing system in the VHF band. It is expected to accommodate numerous wireless systems in a limited spectrum of the VHF band. Consequently, we believe this will lead to the creation of novel applications using the wide-area communication characteristics of the VHF band in the future.

REFERENCES

[1] M. Oodo and H. Harada, "Current status of 200 MHz-band public broadband wireless communication system in Japan," in *Proc. Int. Symp. Wireless Pers. Multimedia Commun.*, Sep. 2014, pp. 759–764.

[2] *200 MHz-Band Broadband Wireless Communication Systems Between Portable BS and MSs*, ARIB STD-T103, Ver. 1.2, Mar. 2015.

[3] *IEEE Standard for Local and Metropolitan Area Networks Part 16: Air Interface for Broadband Wireless Access Systems*, IEEE Standard 802.16TM-2009, May 2009.

[4] K. Makino, K. Mizutani, T. Matsumura, and H. Harada, "A transceiver design of VHF band standard broadband mobile communications systems," in *Proc. 20th Int. Symp. Wireless Pers. Multimedia Commun.*, 2017, pp. 87–93.

[5] H. Harada, K. Makino, K. Mizutani, and T. Matsumura, "A TV white space wireless broadband prototype for wireless regional area network," in *Proc. 21st Int. Symp. Wireless Pers. Multimedia Commun.*, 2018, pp. 206–211.

[6] Assoc. Radio Indust. and Bus., *200 MHz-Band Broadband Wireless Relay Communication Systems Between Portable BS and MSs*, ARIB STD-T119 Ver. 1.2, Oct. 2021. [Online]. Available: https://www.arib.or.jp/english/std_tr/telecommunications/desc/std-t119.html

[7] M. Ishizaki, K. Yamamoto, M. Asano, K. Mizutani, and H. Harada, "Radio sensor development for location estimation using radio big data of ARIB STD-T103/119-compliant wireless communication systems," in *Proc. 24th Int. Symp. Wireless Pers. Multimedia Commun.*, 2021, pp. 1–6.

[8] *IEEE Standard for Information Technology—-Telecommunications and Information Exchange Between Systems Local and Metropolitan area Networks—-Specific Requirements Part 11: Wireless LAN Medium Access Control (MAC) and Physical Layer (PHY) Specifications Amendment 5: Television white Spaces (TVWS) Operation*, IEEE Standard 802.11afTM-2013, Dec. 2013.

[9] K. Mizutani, Z. Lan, and H. Harada, "Time-domain windowing design for IEEE 802.11af based TVWS-WLAN systems to suppress out-of-band emission," *IEICE Trans. Commun.*, vol. E97-B, no. 4, pp. 875–885, Apr. 2014.

[10] K. Mizutani et al., "IEEE 802.11af indoor experiment in U.K. Ofcom TVWS trial pilot program," in *Proc. IEEE 81st Veh. Technol. Conf. (VTC Spring)*, May 2015, pp. 1–5.

[11] T. Matsumura et al., "Prototype of IEEE 802.11af-based baseband IC enabling compact device for wireless local area network systems in TV white-spaces," *IEEE Trans. Cogn. Commun. Netw.*, vol. 3, no. 3, pp. 450–463, Sep. 2017.

[12] *IEEE Standard for Local and Metropolitan Area Networks—-Part 15.4: Low-Rate Wireless Personal Area Networks (LR-WPANs) Amendment 6: TV White Space Between 54 MHz and 862 MHz Physical Layer*, IEEE Standard 802.15.4mTM-2014, Mar. 2014.

[13] C. Sum, L. Lu, M. Zhou, F. Kojima, and H. Harada, "Design considerations of IEEE 802.15.4m low-rate WPAN in TV white space," *IEEE Commun. Mag.*, vol. 51, no. 4, pp. 74–82, Apr. 2013.

[14] J. Ma, H. Harada, and F. Kojima, "Proposal and performance evaluation of TVWS-Wi-SUN system," in *Proc. IEEE 26th Annu. Int. Symp. Pers., Indoor, Mobile Radio Commun.*, 2015, pp. 2002–2007.

[15] *IEEE Standard for Information Technology—-Telecommunications and Information Exchange Between Systems Local and Metropolitan Area Networks—-Specific Requirements Part 22: Cognitive Wireless RAN Medium Access Control (MAC) and Physical Layer (PHY) Specifications: Policies and Procedures for Operation in the Bands that Allow Spectrum Sharing Where the Communications Devices May Opportunistically Operate in the Spectrum of Primary Service*, IEEE Standard 802.22TM-2019, Sep. 2019.

[16] R. Ouyang, T. Matsumura, K. Mizutani, and H. Harada, "A reliable channel estimation scheme using scattered pilot pattern for IEEE 802.22-based mobile communication system," *IEEE Trans. Cogn. Commun. Netw.*, vol. 5, no. 4, pp. 935–948, Dec. 2019.

[17] P. Gronsund, P. Pawelczak, J. Park, and D. Cabric, "System level performance of IEEE 802.22-2011 with sensing-based detection of wireless microphones," *IEEE Commun. Mag.*, vol. 52, no. 1, pp. 200–209, Jan. 2014.

[18] M. Matinmikko et al., "Field trial of licensed shared access (LSA) with enhanced LTE resource optimization and incumbent protection," in *Proc. IEEE Int. Symp. Dynamic Spectr. Access Netw.*, Oct. 2015, pp. 263–264.

[19] J. Milheiro, L. Almeida, J. P. Borrego, N. B. Carvalho, and H. Hokkinen, "LTE signal detector for LSA spectrum sharing model in Portugal," *IEEE Trans. Veh. Technol.*, vol. 69, no. 12, pp. 15127–15136, Dec. 2020.

[20] D. Guiducci et al., "Regulatory pilot on licensed shared access in a live LTE-TDD network in IMT band 40," *IEEE Trans. Cogn. Commun. Netw.*, vol. 3, no. 3, pp. 534–549, Sep. 2017.

[21] M. Weiss, W. Lehr, A. Acker, and M. Gomez, "Socio-technical considerations for spectrum access system (SAS) design," in *Proc. IEEE Int. Symp. Dynamic Spectr. Access Netw.*, Oct. 2015, pp. 35–46.

[22] S. Bhattarai, J. Park, B. Gao, K. Bian, and W. Lehr, "An overview of dynamic spectrum sharing: Ongoing initiatives, challenges, and a roadmap for future research," *IEEE Trans. Cogn. Commun. Netw.*, vol. 2, no. 2, pp. 110–128, Jul. 2016.
[23] M. Sohul, M. Yao, T. Yang, and J. Reed, "Spectrum access system for the citizen broadband radio service," *IEEE Commun. Mag.*, vol. 53, no. 7, pp. 18–25, Jul. 2015.
[24] A. Sakai, K. Mizutani, T. Matsumura, and H. Harada, "Highly efficient sensing methods of primary radio transmission systems toward dynamic spectrum sharing-based 5G systems," *IEICE Trans. Commun.*, vol. E104-B, no. 10, pp. 1227–1236, Oct. 2021.
[25] H. Kuriki, K. Onose, R. Kimura, and R. Sawai, "A new primary protection method with received power-based 3D antenna rotation range prediction for dynamic spectrum access," *IEEE Access*, vol. 9, pp. 74180–74188, 2021.
[26] H. Shinbo, K. Yamazaki, and Y. Kishi, "Research & development of the advanced dynamic spectrum sharing system between different radio services," *IEICE Trans. Commun.*, vol. E104-B, vol. 10, pp. 1198–1206, Oct. 2021.
[27] Int. Telecommun. Union, *Calculation of Free-Space Attenuation*, Recommendation ITU-R P.525-14, Aug. 2019. [Online]. Available: https://www.itu.int/rec/R-REC-P.525/en
[28] *Monte Carlo Simulation Methodology for the use in Sharing and Compatibility Studies Between Different Radio Services or Systems*, Report ITU-R SM.2028-2, Jun. 2017.
[29] *Propagation Data and Prediction Methods for the Planning of Short-Range Outdoor Radiocommunication Systems and Radiolocal Area Networks in the Frequency 300 MHz to 100 GHz*, Recommendation ITU-R P.1411-7 Sep. 2013.
[30] J. Walfish and H. L. Bertoni, "Theoretical model of UHF propagation in urban environments," *IEEE Trans. Antennas Propag.*, vol. 36, no. 12, pp. 1788–1796, Dec. 1988.
[31] F. Ikegami, S. Yoshida, T. Takeuchi, and M. Umehira, "Propagation factors controlling mean field strength on urban streets," *IEEE Trans. Antennas Propag.*, vol. 32, no. 8, pp. 822–829, Aug. 1984.
[32] S. Tomida, K. Mizutani, and H. Harada, "Radio protection area estimation methods for spectrum sharing-based 5G system," in *Proc. IEEE 18th Annu. Consum. Commun. Netw. Conf.*, Jan. 2021, pp. 1–4.
[33] N. Dumont, R. Watson, and S. Pennock, "Validation of a high resolution geolocation database for U.K. white space," in *Proc. 7th Eur. Conf. Antennas Propag.*, Apr. 2013, pp. 2575–2578.
[34] G. Villardi, H. Harada, F. Kojima, and H. Yano, "Primary contour prediction based on detailed topographic data and its impact on TV white space availability," *IEEE Trans. Antennas Propag.*, vol. 64, no. 8, pp. 3619–3631, Aug. 2016.
[35] Int. Telecommun. Union, *Propagation by Diffraction*, Recommendation ITU-R P.526-15, Oct. 2019. [Online]. Available: https://www.itu.int/rec/R-REC-P.526-15-201910-I/en
[36] S. J. Sheather, *A Modern Approach to Regression with R*. New York, NY, USA: Springer, 2009.

KEIKA MINAKI (Student Member, IEEE) received the B.E. degree in electric and electrical engineering in 2022 from Kyoto University, Kyoto, Japan, where he is currently working toward the M.I. degree with the Graduate School of Informatics. His current research focuses on spectrum sharing systems in VHF-band.

SOHEI YANASE was a master course student with the Graduate School of Informatics, Kyoto University, Kyoto, Japan. He received the B.E. degree from the Faculty of Engineering from the Kyoto University, in 2020, and the M.I. degree from Kyoto University, in 2022 . His research focuses on dynamic spectrum sharing technologies. He was the recipient of the Best Paper Award from IEICE SR Technical Committee in 2020.

SHINGO TOMIDA was a master course student with the Graduate School of Informatics, Kyoto University, Kyoto, Japan. He received the B.E. degree from the Faculty of Engineering, Kyoto University, in 2020, and the M.I. degree from Kyoto University, in 2022. His research focuses on dynamic spectrum sharing technologies.

KEIICHI MIZUTANI (Member, IEEE) received the B.E. degree in engineering from Osaka Prefecture University, Sakai, Japan, in 2007, and the M.E and Ph.D. degrees in engineering from the Tokyo Institute of Technology, Tokyo, Japan, in 2009 and 2012, respectively. He is currently an Associate Professor of the Graduate School of Informatics, Kyoto University, Kyoto, Japan. In 2010, he was an Invited Researcher with Fraunhofer Heinrich Hertz Institute, Berlin, Germany. From April 2012 to September 2014, he was a Researcher with the National Institute of Information and Communications Technology (NICT), Tokyo. From October 2014 to December 2021, he was an Assistant Professor of the Graduate School of Informatics, Kyoto University. From January 2021 to September 2022, he was an Associate Professor of the School of Platforms, Kyoto University (KUSP). He is currently Researches the topics of physical layer technologies in white space communications, dynamic spectrum access, wireless smart utility networks (Wi-SUN), and 4G/5G/6G systems including OFDM, OFDMA, MIMO, multi-hop relay network, and full-duplex cellular systems. Since joining in NICT, he has been involved in IEEE 802 standardization activities, namely 802.11af, 802.15.4m and 802.22b. He was the recipient of the Special Technical Awards from IEICE SR technical committee in 2009 and 2017, Best Paper Award from IEICE SR technical committee in 2010 and 2020, Young Researcher's Award from IEICE SRW technical committee in 2016, Best Paper Award from WPMC2017 and WPMC2020, and the Best Paper Presentation Award (1st Place) from IEEE WF-IoT 2020.

HIROSHI HARADA (Member, IEEE) is currently a Professor of the Graduate School of Informatics, Kyoto University, Kyoto, Japan, and an Research Executive Director of Wireless Networks Research Center, National Institute of Information and Communications Technology (NICT). He joined the Communications Research Laboratory, Ministry of Posts and Communications, in 1995 (currently, NICT). He was a Visiting Professor with the University of Electro-Communications, Tokyo, Japan, from 2005 to 2014. Since 1995, he has been researching software defined radio, cognitive radio, dynamic spectrum access network, wireless smart ubiquitous network, and broadband wireless access systems on VHF, UHF, microwave, and millimeter-wave bands. In 2014 he was a Professor of Kyoto University. He has authored the book entitled Simulation and Software Radio for Mobile Communications (Artech House, 2002). He has also joined many standardization committees and forums in the United States and also in Japan and fulfilled important roles for them, especially IEEE 1900 and IEEE 802. He was the Chair of IEEE DySpan Standards Committee and the Vice Chair of IEEE 802.15.4g, IEEE 802.15.4m, 1900.4, and TIA TR-51. He was a Board of Directors of IEEE communication society standards board, SDR forum, DSA alliance, and WhiteSpace alliance. He is a cofounder of Wi-SUN alliance and was the Chairman of the board from 2012 to 2019. He is currently the Vice Chair of IEEE 2857, IEEE 802.15.4aa and Wi-SUN alliance. He moreover was the Chair of the IEICE Technical Committee on Software Radio (TCSR) and the Chair of Public Broadband Mobile Communication Development Committee, ARIB. He is also involved in many other activities related to telecommunications. He was the recipient of the achievement awards in 2006 and 2018 and a Fellow of IEICE in 2009, respectively and the achievement awards of ARIB in 2009, 2018, and 2022, respectively, on the topic of research and development on cognitive radio and wireless smart utility network.